Influence of halo implant on leakage current and sheet resistance of ultrashallow *p*-*n* junctions

V. N. Faifer[a)]
Frontier Semiconductor, 199 River Oaks Parkway, San Jose, California 95134

D. K. Schroder
Department of Electrical Engineering, Arizona State University, Tempe, Arizona 85287-5706

M. I. Current
Frontier Semiconductor, 199 River Oaks Parkway, San Jose, California 95134

T. Clarysse
IMEC, Kapeldreef 75, B-3001 Leuven, Belgium

P. J. Timans
Mattson Technology, Inc., 47131 Bayside Parkway, Fremont, California 94538

T. Zangerle
IMEC, Kapeldreef 75, B-3001 Leuven, Belgium and Applied Sciences Faculty, Université de Liege, B-4000 Liege, Belgium

W. Vandervorst
IMEC, Kapeldreef 75, B-3001 Leuven, Belgium and K.U. Leuven, Electrical Engineering Department, INSYS, Kasteelpark Arenberg 10, B-3001 Leuven, Belgium

T. M. H. Wong
Frontier Semiconductor, 199 River Oaks Parkway, San Jose, California 95134

A. Moussa
IMEC, Kapeldreef 75, B-3001 Leuven, Belgium

S. McCoy and J. Gelpey
Mattson Technology Canada, Inc., 605 West Kent Avenue, Vancouver V6P 6T7, Canada

W. Lerch and S. Paul
Mattson Thermal Products GmbH, 10 Daimlerstrasse, Dornstadt 89160, Germany

D. Bolze
IHP, Im Technologiepark 25, 15236 Frankfurt (Oder) Germany

J. Halim
Frontier Semiconductor, 199 River Oaks Parkway, San Jose, California 95134

(Received 16 May 2006; accepted 23 July 2007; published 16 August 2007)

Sheet resistance and leakage current density of spike rapid thermal processed, millisecond flash annealed, and chemical vapor deposition (CVD) grown ultrashallow junctions (USJs) are compared with the contactless junction photovoltage technique for measurement of sheet resistance and leakage current (R_sL) and four-point probe (4PP) techniques. A significant leakage current increase for USJs formed in halo-implanted profiles is explained by high electron and hole recombination generation in the near-surface end-of-range damaged layer enhanced by trap-assisted tunneling. The reduced thermal budget of millisecond annealing allows junction formation with reduced dopant diffusion and lower sheet resistance. However, when strong halo doping is employed, there is a significant increase in junction leakage current relative to that for junctions formed by spike annealing. This rise in leakage current can be reduced by annealing the halo implants before implanting the USJ or by lowering the halo implant dose. USJs grown with CVD demonstrate low leakage current due to localization of recombination centers at the edge of the depletion layer where recombination (generation) is low. This study demonstrates the importance of characterizing USJs formed in halo profile using the contactless R_sL technique and highlights the limitations of contact probes, such as four-point probes, for characterization of advanced ultralarge scale integrated junctions. © *2007 American Vacuum Society.* [DOI: 10.1116/1.2771552]

[a)]Author to whom correspondence should be addressed; electronic mail: vladimirf@frontiersemi.com

I. INTRODUCTION

The requirement for source-drain extension (SDE) junction depths of <10 nm to control short-channel effects for <30 nm gates[1] has accelerated the development of methods for low-energy implants, activation annealing with peak temperatures >1300 °C for annealing times of <10 ms, low temperature chemical vapor deposition, and new junction monitoring metrology. Millisecond annealing methods, based on scanned laser beams or pulses of light from flash-lamp arrays, are designed to minimize dopant diffusion during annealing.[2] Low temperature chemical vapor deposition (CVD) has also been proposed as a means for forming ultrashallow junctions (USJs) down to the nanometer range.[3] Although millisecond time scale annealings have demonstrated very high levels of dopant activation, combined with minimal diffusion, recent studies have suggested that they do not completely remove all the damage introduced by conventional implant schemes. CVD approaches for USJ formation can lead to high interface state densities and also face many difficult challenges in process integration.[4] Residual damage after millisecond annealings increases the carrier recombination rate and the junction leakage current, especially for USJ formed in combination with highly doped halo profiles.[5] For this reason, the monitoring of leakage current and sheet resistance of USJs formed in halo or highly doped epilayer profiles is important, especially for advanced ultralarge scale integration (ULSI) technology. At the same time, high leakage current density, $>10^{-4}$ A/cm^2, due to band-to-band and trap-assisted tunneling[5–8] makes it very difficult to measure the sheet resistance of USJ formed in highly doped profiles with $N_D > 10^{18}$ cm^{-3} even with advanced nonpenetrating four-point probe measurements (4PP). Leakage current measurements require time-consuming and expensive fabrication of special diodes. For this reason, noncontact monitoring of sheet resistance and leakage current has become very important for fast process control of advanced ULSI technology.

Verkuil developed the first noncontact method and apparatus for the measurement of sheet resistance using photovoltages from two metal rings placed outside an illumination area.[9] The approximate formula that was used for the calculation of the ratio of the relevant photovoltages is valid only for infinitely thin rings. This technique can be used only if the *p-n* junction capacitance is known through measurements by another technique. This disadvantage prevents accurate monitoring of USJs formed in halo and well profiles.

A rigorous two dimensional, frequency-dependent nonsteady-state junction photovoltage (JPV) method was developed in Refs. 10 and 11 and implemented for measuring sheet resistance and leakage current (R_sL method) in *p-n* junctions. The results in Ref. 3 demonstrated that this contactless technique gives measurements with no correlation with standard 4PP measurements but a good correlation with advanced "nonpenetrating" four-point probes, for CVD USJs formed on the top of a medium-doped epilayer (7×10^{17} cm^{-3}), when band-to-band and trap-assisted tunneling is moderate.

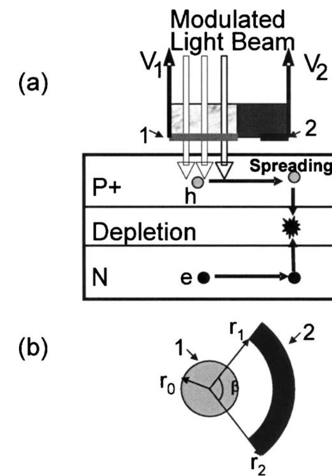

FIG. 1. (a) Photoexcitation and carrier drift with a modulated light source and two capacitor electrodes for monitoring the induced junction photovoltage in a spatially resolved manner and (b) electrode configuration.

This article presents experimental R_sL and 4PP data for spike rapid thermal process (RTP) and flash-assist RTP™ (fRTP™) annealed USJs formed in lightly doped substrates and highly doped ($>10^{18}$ cm^{-3}) halo profiles both with and without Ge ion preamorphization and also for CVD-grown USJs formed on medium-doped (7×10^{17} cm^{-3}) epilayers.

II. MEASUREMENT BACKGROUND

The basis of the R_sL measurement is to use photoexcitation of carriers in the *p-n* junction and wafer substrate and to monitor, in a spatially resolved manner, the JPV signals inside and outside the illumination area, when absorption of a modulated light flux, $\Phi(t)=\Phi_0(1-\cos(2\pi ft))$, creates electron-hole pairs in the semiconductor material. Two electrodes, a circular transparent electrode (1) with diameter $2r_0$ at the center of the probe and a second round arc conducting electrode (2) subtending an angle β and coaxial with the first electrode a small distance away, are used to measure JPV voltages V_1 and V_2 [Figs. 1(a) and 1(b)].[11]

The JPV voltages V_1 and V_2 under low-level excitation are given by Refs. 11 and 12,

$$V_1 = \frac{q\eta(1-R)\Phi_0 R_S}{k^2}[1-2I_1(kr_0)K_1(kr_0)], \tag{1}$$

$$V_2 = q\eta\frac{(1-R)\Phi_0\beta R_S}{\pi k^2 r_0}I_1(kr_0)[r_1K_1(kr_1)-r_2K_1(kr_2)], \tag{2}$$

$$k=\sqrt{R_SG_{p-n}+i2\pi fR_SC_{p-n}}, \tag{3}$$

where I_0, I_1, K_0, and K_1 are modified Bessel functions, Φ_0 the incident photon flux density modulated at frequency f, R, the reflectivity, η the efficiency, and R_S, $G_{p\text{-}n}$, $C_{p\text{-}n}$ the *p-n* junction sheet resistance, capacitance, and conductance. Under illumination, the *p-n* junction is forward biased ($V>0$) and the *p-n* junction voltage at low excitation is $V \ll V_T = kT/q$, where q is the electron charge, k Boltzmann's constant, and T the wafer temperature (K). The junction conduc-

TABLE I. fRTP annealing conditions with intermediate temperature T_i, temperature jump ΔT and peak temperature T_p.

Spike annealing	1050 °C, 100 ppm O_2 in N_2
fRTP A	T_i=700 °C+ΔT=600 °C(T_p=1300 °C)
fRTP B	T_i=700 °C+ΔT=550 °C(T_p=1250 °C)
fRTP C	T_i=750 °C+ΔT=600 °C(T_p=1350 °C)
fRTP D	T_i=750 °C+ΔT=550 °C(T_p=1300 °C)

tance, $G_{p\text{-}n}$, and leakage current density measured using the R_sL method, J_{R_sL}, are defined as

$$G_{p-n} = \left.\frac{dJ}{dV}\right|_{V\to+0} = J_{R_sL}/V_T, \quad (4)$$

where $J(V)$ is the *p-n* junction current density. For an ideal diode,

$$J(V) = J_0[\exp(V/V_T) - 1]. \quad (5)$$

The R_sL leakage current density J_{R_sL} simply equals the prefactor J_0.

By measuring the JPV at the two electrodes at different frequencies, combined with reference JPV measurements on a wafer with a deep *p-n* junction with known sheet resistance, the sheet resistance R_s, conductance $G_{p\text{-}n}$, and capacitance of the *p-n* junction $C_{p\text{-}n}$ can be simultaneously determined using measured voltages V_1 and V_2 and Eqs. (1) and (2).

III. EXPERIMENTS

Millisecond annealings were performed using flash-assisted RTP, where the wafer is rapidly heated to an intermediate temperature and its front surface is then heated further by an ~1.5 ms pulse of energy from a bank of flash lamps.[2] The wafers were (100) oriented, *n* type, and with $\rho > 2\ \Omega$ cm. The study included comparisons of 10^{15} B/cm^2 at 500 eV boron implants into crystalline and amorphous silicon, the effects of halo doping concentration, and the impact of annealing the halo implant before implanting the USJ. The preamorphization implants (PAI) were 10^{15} Ge/cm^2 at 30 keV and the halo implants were 4×10^{13} As/cm^2 at 40 keV. In some samples, the halo implants were annealed for 10 s at 1050 °C before the PAI or B implants. The final annealings were either a spike annealing at 1050 °C or fRTP with a preheating to intermediate temperature T_i followed by a jump to temperature T_p, as given in Table I.

Low temperature CVD boron-doped USJ layers were grown with a doping concentration of about 2×10^{19} cm^{-3} on a 20 μm thick medium arsenic-doped (7×10^{17} cm^{-3}) epilayer grown on an ~10 Ω cm *n*-Si substrate. USJ thickness ranged from 132 nm down to 2 nm.[3]

IV. EXPERIMENTAL RESULTS AND DISCUSSION

We compare R_sL and 4PP sheet resistance data for cases where the leakage current density was $<10^{-4}$ A/cm^2 and also discuss R_sL leakage current data. The results show that

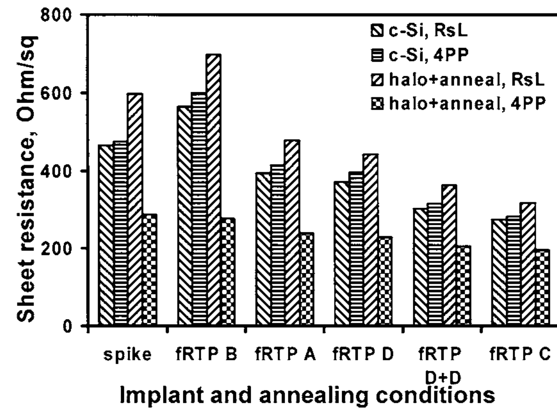

FIG. 2. Noncontact junction photovoltage sheet resistance and leakage current (R_sL) and four-point probe (4PP) sheet resistance for junctions formed by 500 eV implants into crystalline silicon and annealed halo (halo +annealing) that were annealed by spike annealing and flash-assisted thermal process at various conditions (as specified in Table I).

all USJs formed in lightly doped substrates with spike or fRTP annealing, as well as all USJs formed in halo profiles with spike annealing, had leakage current densities below 5×10^{-5} A/cm^2. The leakage current for fRTP annealings of implants with halo implants that had not been preannealed were significantly higher, with $J>10^{-3}$ A/cm^2. For fRTP annealings where the halo was preannealed and preamorphization implants were not performed, $J<5\times10^{-5}$ A/cm^2. For this reason, we compare R_sL and 4PP sheet resistance data for all USJs formed in the lightly doped substrate, for all USJs formed by spike annealing, and for fRTP-annealed USJs formed in preannealed halos.

Figure 2 shows the trends in sheet resistance for USJs after spike or fRTP annealing for the various conditions given in Table I. In this case, the USJs were formed in lightly doped substrates or in preannealed halos. The sheet resistances determined by R_sL demonstrate consistent improvement of activation with increasing annealing temperature. Previous studies have shown that fRTP processing of such implants introduces minimal diffusion, hence providing significant benefits compared to traditional approaches.[13] As was the case for the spike annealings, the 4PP sheet resistances are similar to the R_sL values when the USJs were formed without a halo implant but are significantly lower when the USJs are formed in halo profiles.

Figure 3 compares the R_sL and 4PP sheet resistance data for the selection of USJs discussed here, which only covered cases where the leakage current density was below 10^{-4} A/cm^2. When halo doping is not present the R_sL and 4PP data match closely, but when halo doping is present the 4PP sheet resistances are about two or three times lower than those from the R_sL measurements.

Two factors decrease the sheet resistance determined by the 4PP measurements, intrinsic *p-n* junction leakage and leakage increased by penetration of probes. Figure 4 demonstrates the effect of probe penetration through the dependence of the 4PP sheet resistance on the probe loading force. For USJs formed in preannealed halos, the sheet resistance

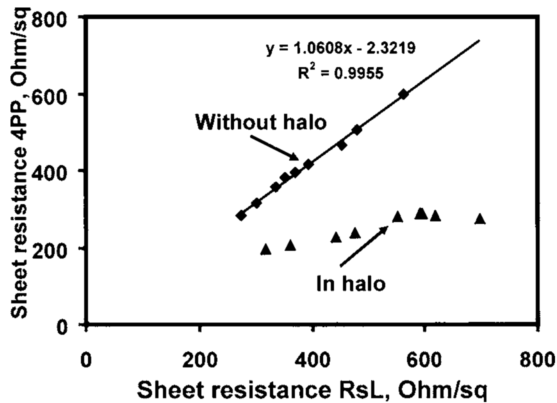

FIG. 3. Comparison of sheet resistance values from four-point probe technique vs noncontact sheet resistance and leakage current (R_sL) measurements for ultrashallow junctions with leakage current density $<5 \times 10^{-5}$ A/cm^2 formed in lightly doped substrate (without halo) and halo profile (with halo).

measured by the 4PP rises as the probe loading force, and hence the probe penetration, decreases. In contrast, for USJs formed in lightly doped substrates without halo doping, the sheet resistance is nearly independent of the loading force. For leaky *p-n* junctions, there are substantial substrate currents flowing below the USJ layer and the 4PP sheet resistance is close to that of the substrate and dose not depend on load force. However, decreasing the loading force makes the 4PP measurements difficult to reproduce, leading to increased variance in the measurements and more than 50% of the values in the 4PP sheet resistance map being reported as errors.

Figure 5 shows the junction leakage current trends for several conditions. Spike annealings give consistently low leakage current, regardless of the implant scheme, probably because of the larger thermal budget allowing defects to be eliminated, combined with the effects of dopant diffusion on the location of the junction relative to the residual implant damage layer.[14] The leakage current density for implants without halo doping was below the measurement limit of

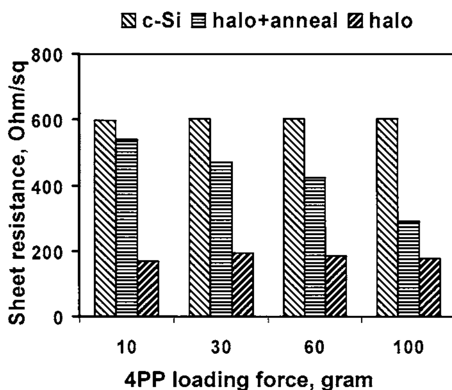

FIG. 4. Four-point probe sheet resistance vs probe loading force for ultrashallow junctions (USJs) without halos in lightly doped substrates (*c*-Si) and for USJs formed in halos that have been preannealed (two types of junction that show low leakage) and for USJs formed in unannealed halos (junctions that show high leakage).

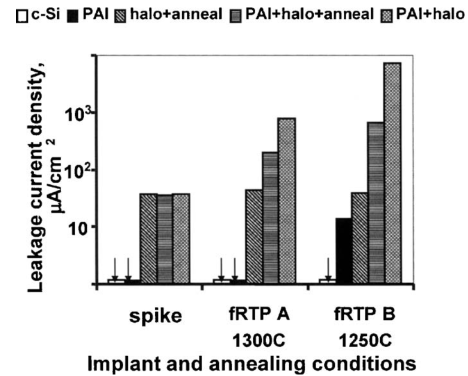

FIG. 5. Leakage current density for junctions formed by 500 eV boron implants into various samples, annealed by various methods.

0.1 μA/cm^2, except for the case of fRTP at 1250 °C with Ge PAI damage. The presence of halo doping consistently increases the leakage current because of the greatly reduced depletion layer width and the overlap of the peak recombination rates with the residual implant damage distribution[10] and the effects of trap-assisted tunneling.[11] Annealing the halo implant damage prior to the B doping steps significantly improved the leakage current. Ge PAI damage resulted in significant leakage current after fRTP annealing at 1250 °C, but 1300 °C annealings were more effective in reducing leakage currents.

These results illustrate that optimization of millisecond annealing demands simultaneous tuning of the halo doping condition as well as the thermal budget employed. The reduced thermal budget in the fRTP annealing can lead to residual defects.[15] The leakage current in halo-doped cases can then be significantly higher than that for spike annealing, even if no leakage current degradation is seen in non-halo-doped cases. The halo doping condition must be carefully optimized to take account of this effect. One simple approach is to reduce the halo dose, which should be possible, because the greatly reduced dopant diffusion with fRTP naturally tends to suppress short-channel effects, moderating the need for strong halo doping.[16] Preliminary annealing of halo damage prior to B doping also decreases the leakage current.

Figure 6 shows the R_sL inverse sheet resistance and junction leakage current density versus junction depth for CVD-

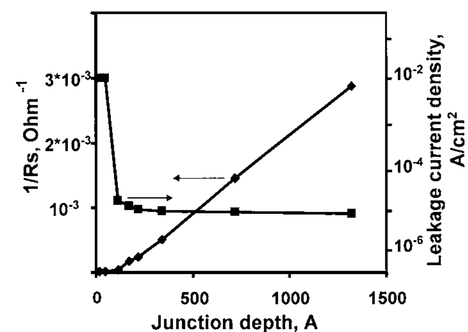

FIG. 6. Inverse sheet resistance and leakage current density vs layer thickness for ultrashallow junctions formed by chemical vapor deposition.

grown USJ. Significant increases of leakage current and sheet resistance, exceeding the upper limits for R_sL measurements (10^{-2} A/cm^2, 10^5 Ω/sq), are observed only for USJs with x_i=1.7 nm and x_j=4.8 nm. In agreement with C-V data, these USJs do not have p-n junctions.[3] The intercept of the $1/R_s$ trend at ~10 nm indicates that the CVD growth process resulted in an inactive dopant layer of ~10 nm for all layers, corresponding to the high R_s (>10^5 Ω/sq) and high leakage current for x_j<10 nm shown in Fig. 5.[3] For CVD layers thinner than 10 nm, the lack of p-n junction activity, reflected in the R_sL measurements through the lack of strong JPV signals and high R_s and leakage currents, could be due to either structural defects incorporated during the initial stage of the growth process or depletion effects from charged states at the growth interface, or from a combination of these effects.

V. CONCLUSION

This study demonstrates the importance of characterizing USJs formed in halo profiles for 65 and 45 nm ULSI. The results reveal the challenges remaining for incorporation of millisecond time scale annealing for complementary metal-oxide semiconductor fabrication and highlight the importance of basing process choices on accurate quantitative information regarding dopant activation and leakage currents for highly doped multiprofile junctions. Significantly higher leakage currents are observed for USJ formed in highly doped halo profiles due to high carrier recombination-generation rates increased by trap-assisted tunneling.

The opportunities for process optimization can be seen in the systematic improvements in leakage currents that are observed with R_sL measurements for USJs formed in halo profiles where the As implant damage has been reduced by annealing prior to the B doping steps. Optimization of USJ formation using advanced annealing requires careful balance of halo "strength" and shallow junction doping, balancing control of short-channel effects with leakage currents. Accurate process monitoring of USJs formed with millisecond time scale annealing requires the inclusion of a comprehensive set of interacting implant profiles and thermal processing conditions (halo, PAI, SDE, and annealings) in order to provide reliable guidance for process decisions. The challenges posed by the thin (~10 nm) dopant layers and high leakage current densities (>10^{-4} A/cm^2), which are characteristic of these combined profiles, rule out the use of contact probes, such as four-point probes, and favor the use of noncontact measurements of sheet resistance and leakage current, provided by R_sL methods.

ACKNOWLEDGMENTS

The authors acknowledge Ann Koo for support of this project and V. Souchkov for his contribution.

Presented at the AVS 53rd International Symposium & Exhibition, 12–17 November 2006, San Francisco, CA.

[1]See Table 69 in the Front End Process section of the ITRS05 (www.itrs.net).
[2]P. Timans *et al.*, Mater. Res. Soc. Symp. Proc. **912**, 0912-C01-01 (2006).
[3]T. Clarysse *et al.*, Mater. Res. Soc. Symp. Proc. **912**, 0912-C05-07 (2006).
[4]M. Mansoori, A. Jain, D. E. Mercer, L. Robertson, and P. Kohli, Proc.-Electrochem. Soc. **2000-11**, 389 (2002).
[5]R. Lindsay *et al.*, J. Vac. Sci. Technol. B **22**, 306 (2004).
[6]P. M. Solomon, D. J. Frank, J. Jopling, C. D'Emic, O. Dokumaci, P. Ronsheim, and W. E. Haensch, Tech. Dig. - Int. Electron Devices Meet. **2003**, 9.3.1.
[7]J. E. Park, J. Shields, and D. K. Schroder, Solid-State Electron. **47**, 855 (2003).
[8]E. C. Jones and N. W. Cheung, J. Vac. Sci. Technol. B **14**, 236 (1996).
[9]Roger L. Verkuil, U.S. Patent No. 5,442,297 (1995).
[10]V. N. Faifer, M. I. Current, T. M. H. Wong, and V. V. Souchkov, J. Vac. Sci. Technol. B **24**, 414 (2006).
[11]V. N. Faifer, D. K. Schroder, and M. I. Current, Appl. Phys. Lett. **89**, 151123 (2006).
[12]T. Clarysse, A. Moussa, F. Schaus, W. Vandervorst, V. N. Faifer, and M. I. Current, Proceeding of INSIGHT-07 Workshop, Napa, CA, 2007 (unpublished), p. 263.
[13]W. Lerch *et al.*, Mater. Sci. Eng., B **124–125**, 24 (2005).
[14]S. Paul, W. Lerch, X. Hebras, N. Cherkashin, and F. Cristiano, Mater. Res. Soc. Symp. Proc. **810**, C5.4.1 (2004).
[15]W. Lerch *et al.*, ECS Trans. **3**, Issue 2, 77 (2006).
[16]F. Ootsuka *et al.*, Tech. Dig. - Int. Electron Devices Meet. **2003**, 647.